Spirochete antigens persist near cartilage after murine Lyme borreliosis therapy

Linda K. Bockenstedt,[1] David G. Gonzalez,[2] Ann M. Haberman,[2] and Alexia A. Belperron[1]

[1]Department of Internal Medicine and [2]Department of Laboratory Medicine, Yale University School of Medicine, New Haven, Connecticut, USA.

An enigmatic feature of Lyme disease is the slow resolution of musculoskeletal symptoms that can continue after treatment, with some patients developing an inflammatory arthritis that becomes refractory to antibiotic therapy. Using intravital microscopy and the mouse model of Lyme borreliosis, we observed that *Borrelia burgdorferi* antigens, but not infectious spirochetes, can remain adjacent to cartilage for extended periods after antibiotic treatment. *B. burgdorferi* was not recovered by culture or xenodiagnosis with ticks after antibiotic treatment of WT mice and all but one of the immunodeficient mice with heightened pathogen burden due to impaired TLR responsiveness. Amorphous GFP$^+$ deposits were visualized by intravital microscopy in the entheses of antibiotic-treated mice infected with GFP-expressing spirochetes and on the ear cartilage surface in sites where immunofluorescence staining detected spirochete antigens. Naive mice were not infected by tissue transplants from antibiotic-treated mice even though transplants contained spirochete DNA. Tissue homogenates from antibiotic-treated mice induced IgG reactive with *B. burgdorferi* antigens after immunization of naive mice and stimulated TNF-α production from macrophages in vitro. This is the first direct demonstration that inflammatory *B. burgdorferi* components can persist near cartilaginous tissue after treatment for Lyme disease. We propose that these deposits could contribute to the development of antibiotic-refractory Lyme arthritis.

Introduction

Lyme disease is an emerging zoonotic infection caused by the *Ixodes* tick–transmitted spirochete *Borrelia burgdorferi* (1). Spirochetes deposited in the skin during tick feeding can cause the localized skin rash erythema migrans (EM) or disseminate to cause disease mainly involving other areas of the skin and/or the heart, joints, and nervous system. Although the disease is responsive to antibiotics, up to 25% of patients treated early in the course of infection can experience protracted musculoskeletal symptoms of unclear etiology (2). Patients who present with the late-stage manifestation of arthritis may evolve persistent joint inflammation that no longer responds to antibiotics (3). Although ongoing infection is considered an unlikely explanation for persistent symptoms or disease, it cannot be definitively excluded because *B. burgdorferi* is difficult to detect by culture except in early infection when EM is present (4). The pathogenic mechanisms underlying the delay in symptom resolution after treatment for early disease and the persistence of objective late signs such as arthritis are incompletely defined.

The mouse model of Lyme borreliosis has provided a useful system for studying *B. burgdorferi* infection in mammals (5). All laboratory mice are susceptible to infection and develop subacute arthritis and myocarditis similar to that of humans infected with *B. burgdorferi*. Disease severity is mouse strain dependent, with C3H mice more susceptible than C57BL/6 (B6) mice. Strain differences in disease susceptibility are influenced by both hematopoietic and nonhematopoietic factors and are preserved in SCID mice that lack functional T and B cells (6, 7). Effective pathogen control requires both specific Ab production and phagocyte recognition of *B. burgdorferi* via TLRs, as demonstrated by the markedly elevated pathogen burdens in mice deficient in B cells, in TLR2, or in the TLR intracellular adaptor molecule myeloid differentiation antigen 88 (MyD88) (8–11). Adaptive immunity is required for resolution of joint inflammation, which usually occurs within 45–60 days of infection even though spirochetes persist in tissues throughout the life span of the mouse (5, 8, 10).

Our laboratory and others have used the C3H mouse model of Lyme borreliosis to evaluate whether viable *B. burgdorferi* can persist after antibiotic treatment (12–14). Using xenodiagnosis with ticks, we showed that spirochetes could be detected for up to 3 months after treatment with either ceftriaxone or doxycycline for *B. burgdorferi* infection introduced by tick bite (14). Spirochetes acquired by ticks that were recovered from antibiotic-treated mice lacked genes on plasmids lp25 and lp28-1 associated with infectivity, suggesting that they were attenuated. Nymphs derived from a group of larval ticks that tested positive for *B. burgdorferi* plasmid DNA after feeding on antibiotic-treated mice could not transmit infection to naive mice. Spirochetes were not cultured from antibiotic-treated mice, even after immunosuppression with cortisone, but low levels of *B. burgdorferi* DNA were detected by PCR in multiple tissues. A subsequent study examined efficacy of ceftriaxone administered to C3H mice 3 weeks or 4 months after *B. burgdorferi* infection introduced by needle inoculation (13). Some larval ticks used for xenodiagnosis acquired spirochete DNA from antibiotic-treated mice and, after molting to nymphs, transmitted *B. burgdorferi* DNA to a small proportion of SCID mice used as blood meal hosts. Rare spirochete-like forms could be detected by immunohistochemistry in connective tissue of the heart and tibiotarsal joints of antibiotic-treated mice, but spirochetes could not be cultured from these tissues. Taken together, these findings suggest that attenuated, noncultivable spirochetes could persist at low levels in mice after antibiotic treatment for disseminated *B. burgdorferi* infection.

In this study, we used the elevated pathogen burden in *B. burgdorferi*–infected *Myd88*$^{-/-}$ mice and intravital 2-photon microscopy to further investigate spirochetes that may persist after antibiotic therapy. Our results show that infectious spirochetes are rapidly eliminated after institution of antibiotics, but inflammatory *B. burgdorferi* antigens persist adjacent to cartilage and in the entheses.

Conflict of interest: The authors have declared that no conflict of interest exists.

Citation for this article: *J Clin Invest.* doi:10.1172/JCI58813.

Table 1
Oral doxycycline eliminates cultivable BbN40 from WT and most *Myd88*$^{-/-}$ mice

Mouse group	Culture of mouse tissue[A,B]	*B. burgdorferi* DNA in mouse tissue[A]		Culture of xenodiagnostic ticks[A]	*B. burgdorferi* DNA in xenodiagnostic ticks[A]
		Joints (*ospA*)	Skin (*16S rRNA*)		
WT sham	3/3	3/3	3/3	3/3	3/3
WT doxycycline	0/5	0/5	1/5	0/5	0/5
WT uninfected	0/2	0/2	0/2	0/2	0/2
Myd88$^{-/-}$ sham	3/3	3/3	3/3	2/3	3/3
Myd88$^{-/-}$ doxycycline	1/12[C]	12/12	5/12[C]	1/12[D]	1/12[C,D]
Myd88$^{-/-}$ uninfected	0/2	0/2	0/2	0/2	0/2

[A]Results are reported as the number of mice testing positive over the total number of mice examined. [B]Results are from cultures of urinary bladders, ear skin, and tibiotarsal joints. [C]Differences between doxycycline-treated and sham-treated *Myd88*$^{-/-}$ mice are significant ($P = 0.0088$, Fisher's exact test). [D]The mouse testing positive for infection by culture also tested positive by xenodiagnosis with ticks.

We believe this is the first direct demonstration that inflammatory *B. burgdorferi* components can persist for extended periods after resolution of *B. burgdorferi* infection, and it raises the possibility that these spirochete remnants contribute to the pathogenesis of antibiotic-refractory Lyme arthritis.

Results

B. burgdorferi DNA can be detected in B6 Myd88$^{-/-}$*, but not WT, mice after treatment with doxycycline*. To determine whether persistence of *B. burgdorferi* observed in antibiotic-treated C3H mice could be demonstrated in the disease-resistant B6 background, we infected cohorts of B6 WT and *Myd88*$^{-/-}$ mice with *B. burgdorferi* strain N40 (BbN40) by tick bite. Infection was confirmed by *B. burgdorferi* immunoblot (data not shown). At 30 days after infection, mice were treated with doxycycline administered continuously in drinking water to sustain serum drug levels above the mean inhibitory concentration (MIC) for *B. burgdorferi* during the treatment period (see Methods). Xenodiagnosis with ticks was performed at 1, 4, and 7 weeks after the last day of treatment. At the end of the 15-week experimental period (9 weeks after completion of antibiotics), no spirochetes were detected in doxycycline-treated WT mice by culture or xenodiagnosis with ticks (Table 1). *B. burgdorferi* was cultured from 1 of 12 *Myd88*$^{-/-}$ mice treated with doxycycline, and ticks that fed on the infected mice tested positive for *B. burgdorferi* by culture and PCR. *B. burgdorferi* could not be cultured from blood or tissues of the remaining 11 doxycycline-treated *Myd88*$^{-/-}$ mice or from ticks that fed on those mice, but spirochete plasmid DNA (*ospA*) could be detected in the knee joints of all the mice (Table 1). Ear-skin samples tested positive for *B. burgdorferi* DNA in almost half of the doxycycline-treated *Myd88*$^{-/-}$ mice and in only 1 of 5 doxycycline-treated WT mice. As expected, sham-treated mice showed evidence of spirochetes by all parameters examined, including culture, whereas uninfected controls tested negative.

Real-time imaging of B. burgdorferi in Myd88$^{-/-}$ *mice reveals rapid spirochete elimination after antibiotic therapy*. To begin to assess whether DNA in tissue could represent a subpopulation of live spirochetes that remained after antibiotic therapy, we used intravital 2-photon microscopy to image in real time the immediate effects of antibiotics on spirochetes in living mice. *Myd88*$^{-/-}$ mice infected for 21 days with a transformant of *B. burgdorferi* strain 297 expressing a GFP reporter protein under the control of the *flaB* promoter (Bb914) (15) were treated with a 5-day course of ceftriaxone or were sham treated. Ceftriaxone was chosen for its bactericidal effects, which could lead to changes in *B. burgdorferi* more rapidly than doxycycline, a bacteriostatic agent (16). We visualized numerous highly motile spirochetes in the dermis of sham-treated mice (Figure 1A and Supplemental Video 1; supplemental material available online with this article; doi:10.1172/JCI58813DS1); spirochetes were fewer in number and moved more slowly in the calcaneal tendon at all time points analyzed (Figure 1C and Supplemental Video 2). Motility patterns of spirochetes within a field varied, with the majority of spirochetes moving back and forth in tracks along collagen fibers and others

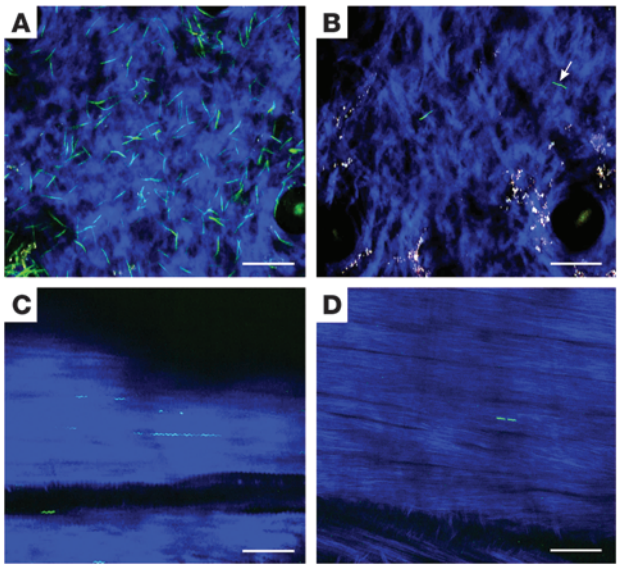

Figure 1
Ceftriaxone reduces pathogen burden in *Myd88*$^{-/-}$ mice within 24 hours of therapy. (**A**) Image from Supplemental Video 1 of Bb914 in ear skin of sham-treated *Myd88*$^{-/-}$ mouse at 22 days of infection. Blue, second harmonics of skin collagen. (**B**) Still image from Supplemental Video 3 of Bb914 in *Myd88*$^{-/-}$ mouse after 1 day of ceftriaxone. Arrow denotes the spirochete tracked in Figure 2. White, melanin fluorescence. (**C**) Image of Bb914 aligned with tendon fibers of a sham-treated *Myd88*$^{-/-}$ mouse. Spirochete length variation may be due to spirochetes in tandem or immediately after replication. See also Supplemental Video 2. (**D**) Image of Bb914 in the tendon of a *Myd88*$^{-/-}$ mouse after 1 day of ceftriaxone. These spirochetes did not exhibit detectable movement. Scale bars: 60 μm.

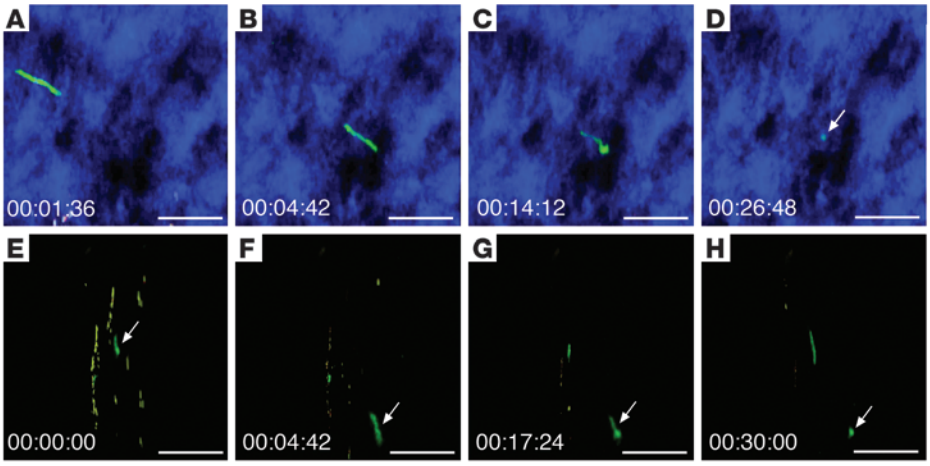

Figure 2
Image sequences of Bb914 changing from an elongated spirochete to a spherical form. The spirochete image is labeled with an arrow in Figure 1B. (**A**–**D**) Images in the *xy* plane from Supplemental Video 3 depicting changes in morphology of Bb914 over time; arrow (**D**) shows the spherical form. (**E**–**H**) Images from Supplemental Video 4 showing the same spirochete (arrows) imaged in **A**–**D** in the *yz* plane. The blue channel has been suppressed. Scale bars: 30 μm.

exhibiting more directional translocation. Less frequently, spirochetes undulated as a traveling wave without positional displacement. We have observed similar patterns of motility in infected WT mice (17). At 24 hours after instituting antibiotics, the population of spirochetes had diminished dramatically in the dermis and tendons (Figure 1, B and D). Remaining spirochetes in the dermis but not the tendon appeared motile, and continuous imaging captured 2 events in which these spirochetes rapidly transformed into spherical objects. In one case, a motile spirochete abruptly stopped and became spherical within the 30-minute observation period (Figure 2 and Supplemental Videos 3 and 4). In the second case, a spirochete appeared to be tethered at one end and initially wriggling in place (Supplemental Video 5). Continuous imaging revealed that the spirochete flexed once and then rapidly converted into a spherical shape. After imaging at the 1-day time point, we were unable to visualize spirochetes in the skin or tendons of ceftriaxone-treated mice by this technique.

Spirochete antigens can be detected adjacent to ear cartilage in antibiotic-treated Myd88$^{-/-}$ mice. At the end of the experimental period, all sham-treated mice tested positive for *B. burgdorferi* by both culture of tissues and direct immunofluorescence staining using FITC-conjugated anti–*B. burgdorferi* Ab (DFA) of ear-skin cryosections, which revealed spirochetes throughout the dermis (Table 2 and Figure 3A). Although spirochetes were not cultured from any of the ceftriaxone-treated mice, DFA detected spirochete antigens in the deep dermis adjacent to ear cartilage (Figure 3, B and C); their location was deeper than the level at which intravital imaging had been performed. Residual spirochete antigens also were seen by DFA of ear sections from the BbN40-infected *Myd88*$^{-/-}$ mice treated with doxycycline described above (Figure 3E). None of the antibiotic-treated tissues contained cultivable spirochetes. Negative cultures suggested that if immunofluorescence staining represented viable spirochetes, the residual organisms were deficient in their ability to multiply when transferred to the culture environment.

Live imaging reveals antigen deposits but not motile spirochetes adjacent to cartilage of Myd88$^{-/-}$ mice after doxycycline treatment for B. burgdorferi infection. To further assess the significance of DFA detection of spirochete antigens, we conducted a third experiment in which Bb914-infected *Myd88*$^{-/-}$ mice were evaluated between 2 and 10 weeks after completion of a 1-month course of oral doxycycline (Table 3). Xenodiagnosis with ticks was performed prior to mouse sacrifice, and *B. burgdorferi* DNA was amplified from some ticks that had fed on doxycycline-treated mice. DFA of tick midgut contents, however, did not reveal spirochetes in ticks that acquired blood meals from antibiotic-treated mice, nor were spirochetes cultured from the ticks; only sham-treated mice tested positive for viable *B. burgdorferi* by these modalities (Table 3). As in our previous experiment with BbN40-infected mice, spirochetes could not be cultured from any of the antibiotic-treated mice, but residual spirochete antigens were detected by DFA adjacent to ear cartilage at all time points examined. Using live imaging parameters to include the level of the ear cartilage, we observed that sham-treated mice had not only motile spirochetes in the dermis extending to the cartilage surface, but also large amorphous deposits of nonmotile fluorescent material at the dermal-cartilage interface (Figure 4A and Supplemental Video 6). Similar GFP^{+} deposits, but not morphologically intact or motile spirochetes, were visualized adjacent to ear cartilage in all doxycycline-treated mice (Figure 4B). This mate-

Table 2
Ceftriaxone eliminates cultivable Bb914 from *Myd88*$^{-/-}$ mice

Mouse group	Culture of mouse tissue[A,B]	DFA of tissues for *B. burgdorferi*[A]				Multiphoton imaging[A]	
		Ear skin	Heart	Tibiotarsal joint	Achilles tendon	Ear skin	Tendon
Sham	3/3	3/3	2/3	3/3	3/3	3/3	3/3
Ceftriaxone	0/6[C,D]	6/6	0/6	0/6[D]	0/6[D]	2/6[C]	1/6[C,E]

[A]Results are reported as the number of mice that had positive cultures for *B. burgdorferi* over the total number of mice examined. [B]Results are from cultures of urinary bladders, ear skin, and tibiotarsal joints. [C]The mice testing positive for *B. burgdorferi* by multiphoton imaging were evaluated at day 1 after ceftriaxone therapy, and tissues harvested for culture were collected within 1 hour after administration of a third dose of ceftriaxone. [D]Differences between sham- and ceftriaxone-treated mouse groups were statistically significant ($P = 0.0119$, Fisher's exact test, for all comparisons). [E]Differences between sham- and ceftriaxone-treated mouse groups were statistically significant ($P = 0.0476$, Fisher's exact test).

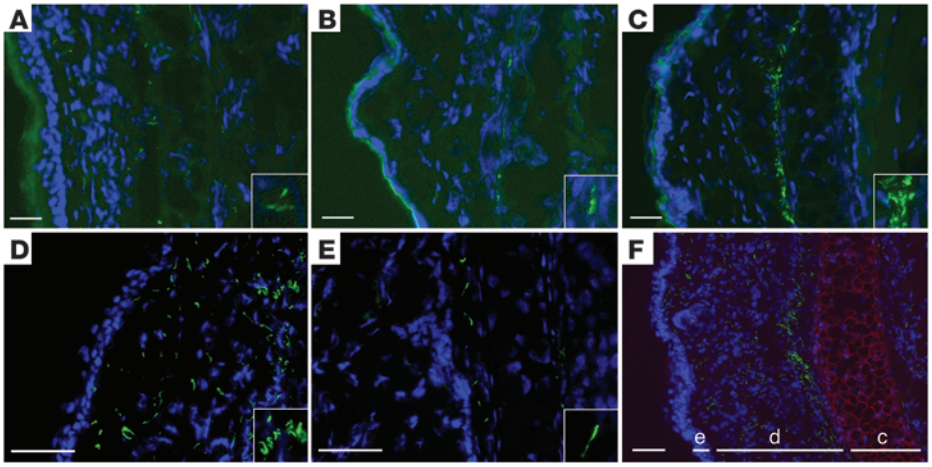

Figure 3
DFA of ear skin cryosections from sham- and antibiotic-treated *Myd88*$^{-/-}$ mice. Sagital sections show spirochetes (green) detected with FITC-conjugated anti–*B. burgdorferi* Ab and DAPI (blue) delineating cell nuclei. Acetone fixation eliminates GFP expressed by Bb914. **A**–**C** are representative of sham-treated (**A**) and ceftriaxone-treated Bb914-infected mice (**B** and **C**). **D**–**F** are representative of sham-treated (**D** and **F**) and doxycycline-treated BbN40-infected mice (**E**). The epidermis (e), dermis (d), and cartilage (c) are labeled in **F**; autofluorescence of the cartilage is detected in the red channel. *B. burgdorferi* is present in the dermis and adjacent to the cartilage in all sham-treated mice. Antibiotic-treated mice only had *B. burgdorferi* antigens detected at the dermal-cartilage interface, with significant variation in amount from mouse to mouse. Scale bars: 50 μm.

rial was only found at imaging depths corresponding to the regions viewed sagitally on ear-skin cryosections that tested positive by DFA (Figure 3). As further evidence that infectious spirochetes had been eliminated by antibiotic treatment, only transplanted ear skin from sham-treated mice introduced infection into naive *Myd88*$^{-/-}$ mice, as documented by IgG seroconversion to multiple *B. burgdorferi* antigens and culture (Supplemental Figure 1A). In contrast, similar transplants from antibiotic-treated mice induced reactivity to only 1 or 2 *B. burgdorferi* antigens, and spirochetes were not cultured from recipient mice (Supplemental Figure 1, A and B). This pattern of reactivity was reproduced when mice were immunized with homogenates of sham-treated mouse ears (Supplemental Figure 1C).

Spirochete antigens can be detected in joints of antibiotic-treated C3H Myd88$^{-/-}$ *mice*. Because *B. burgdorferi* DNA was detected in the joints of antibiotic-treated mice, we postulated that this site could also contain deposits of *B. burgdorferi* antigens. Subsequent to the above studies, we developed a technique to image the articular surfaces and adjacent entheses of the patellofemoral joint. Striking amounts of GFP deposits as well as motile spirochetes were seen by intravital microscopy in the patellae entheses in 4-month–infected C3H *Myd88*$^{-/-}$ mice (Figure 5A and Supplemental Video 7). Treatment of mice with ceftriaxone (used to image the immediate effects of the treatment on chronically host-adapted spirochetes) eliminated motile spirochetes but not the debris (Figure 5B). Spirochetes were not cultured from any antibiotic-treated mouse.

Tissues from antibiotic-treated mice contain immunogenic and inflammatory B. burgdorferi antigens. To provide further support that the GFP deposits contained spirochete antigens, we immunized groups of mice with homogenates of patellar tissue from sham- or ceftriaxone-treated mice. Both tissues used as immunogens resulted in IgG seroconversion to several *B. burgdorferi* proteins (Figure 6A), whereas tissues from uninfected mice induced only weak reactivity to a protein band of approximately 41 kDa protein. In addition, IgG from infected mice bound antigens present in patella homogenates of sham- and antibiotic-treated mice (Figure 6B). These antigens had molecular weights similar to those detected on *B. burgdorferi* immunoblots (Figure 6B). Homogenates of patellar tissue from both sham- and ceftriaxone-treated mice induced TNF-α production from C3H/HeJ macrophages in vitro (Figure 7). Ear skin of sham-treated mice contained insufficient amounts of spirochetal antigens to stimulate production of TNF-α from macrophages in vitro (data not shown).

Discussion

This study demonstrates that antibiotics (ceftriaxone or doxycycline) eliminate infectious *B. burgdorferi* from mice with disseminated infection, even when the host is immunocompromised and initially has a high pathogen burden. Through use of *Myd88*$^{-/-}$ mice and intravital microscopy, we have shown that ceftriaxone rapidly (within 24 hours) reduces pathogen burden in the skin, a preferential site of *B. burgdorferi* infection, and that both ceftriaxone and doxycycline eliminate infectious spirochetes as assessed by real-

Table 3
Doxycycline eliminates cultivable Bb914 from *MyD88*$^{-/-}$ mice

Mouse group	Culture of mouse tissue[A,B]	*ospA* PCR from mouse tissues[A]	DFA of mouse tissues[A]	Culture of xenodiagnostic ticks[A,C]	*ospA* PCR from xenodiagnostic ticks[A]	DFA of tick midguts[A]
Sham	4/4	4/4	4/4	4/4	5/5	5/5
Doxycycline	0/9[D]	3/8[D]	9/9[E]	0/7	7/8	0/7[D]

[A]Results are reported as the number of mice that had positive cultures for *B. burgdorferi* over the number of mice examined. [B]Results are from cultures of urinary bladders, ear skin, and one tibiotarsal joint. One mouse from each group died during tick feeding; ticks were retrieved from the sham-treated mouse for analysis. [C]Ticks placed on mice 2 weeks after sham or doxycycline treatment were not analyzed by culture, PCR, or DFA for *B. burgdorferi*. [D]Results from doxycycline-treated mice were significantly different from those of sham-treated mice (Fisher's exact test, $P = 0.0014$ for comparison of mouse tissue culture; $P = 0.0256$ for comparison of *B. burgdorferi* DNA in mouse tissues; $P = 0.0013$ for comparison of DFA of tick midguts). [E]Ear skin of doxycycline-treated mice exhibited immunofluorescence staining adjacent to ear cartilage, but not in the dermal connective tissue.

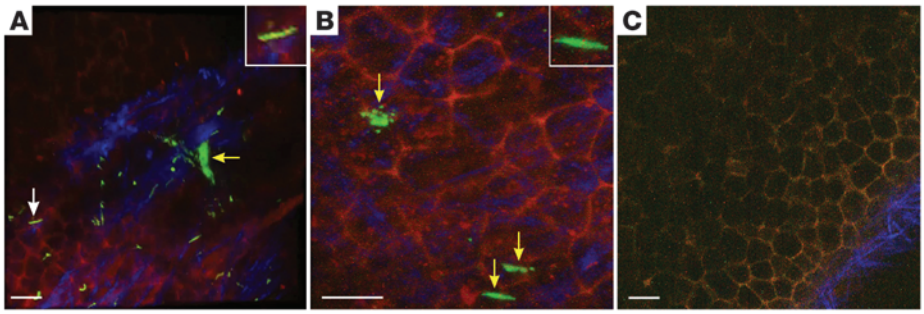

Figure 4
Amorphous GFP deposits on the dermal-cartilage interface of Bb914-infected mice. (**A**) Multiphoton image of typical GFP+ spirochete (white arrow and inset) and amorphous GFP deposits (yellow arrow) on the surface of ear cartilage (red) of Bb914-infected mouse (see also Supplemental Video 6). (**B**) Multiphoton image of a doxycycline-treated mouse ear showing GFP deposits (yellow arrows), but not typical spirochete forms (see also inset). (**C**) Multiphoton image of the dermal-cartilage interface of an uninfected mouse. The green channel was enhanced to show absence of fluorescent green deposits. Images were acquired using a ×20 objective and optically zoomed to a scanned field of view of 300 × 300 μm in **A** and **C** and 150 × 150 μm in **B**. The objects delineated by arrows in **A** and **B** are enlarged 3-fold and 1.7-fold, respectively, in the corresponding insets. Scale bars: 30 μm.

time imaging, culture, and xenodiagnosis with ticks. Our studies also provide what we believe is the first direct evidence that spirochete remnants can persist adjacent to ear cartilage and within joint entheses. Notably, these remnants contain immunogenic material that can induce IgG responses to *B. burgdorferi* antigens in naive recipients and stimulate macrophages to produce TNF-α in vitro.

Previous studies examining antibiotic efficacy in murine Lyme borreliosis used the BbN40 strain (12–14). Here, we found that antibiotics were effective against 2 strains of *B. burgdorferi* (BbN40 and Bb914) that represent genotypes that differ in their capacity for dissemination and pathogenicity (18, 19). Improved efficacy of doxycycline in WT mice as compared with that found in previous studies may be due to its administration in drinking water, which optimizes the time interval for which serum drug levels remain above the MIC for *B. burgdorferi* (20). With the exception of a single doxycycline-treated *Myd88*$^{-/-}$ mouse, cultivable spirochetes were eliminated from all antibiotic-treated *Myd88*$^{-/-}$ mice infected with either *B. burgdorferi* strain. Presence of infection in 1 of a total of 21 *Myd88*$^{-/-}$ mice was easily demonstrated by several modalities, including culture of mouse tissues and the ticks used for xenodiagnosis. This contrasts with our earlier report, in which intact organisms were documented only by xenodiagnosis in a subset of doxycycline-treated animals (14). Administration of doxycycline by gavage twice daily results in periods in which serum drug levels fall below the MIC for BbN40, which may allow for the persistence of attenuated, noncultivable organisms (21). The failure of antibiotics to eliminate *B. burgdorferi* from a single *Myd88*$^{-/-}$ mouse may have been due to a drinking pattern that led to inconsistent doxycycline levels.

The significance of *B. burgdorferi* DNA in xenodiagnostic ticks and in mouse tissues after antibiotic therapy is unclear. The nymphs used in the study were from a specific pathogen–free colony derived from larvae that fed on uninfected laboratory mice; the colony was routinely tested for *B. burgdorferi* by PCR. In humans, spirochete DNA has been detected by PCR for up to 9 months after treatment for Lyme arthritis, but its presence does not correlate with relapse or duration of arthritis (22). Microbial DNA can persist in mammalian tissues for extended periods (years) when sequestered in cellular debris even though the microbe itself is no longer viable (23, 24). Some *B. burgdorferi* DNA could remain intact if it is sequestered in cellular debris such as the GFP deposits. Alternatively, spirochete DNA could represent a minor subpopulation of *B. burgdorferi* that is not killed by the antibiotic treatment.

It has been proposed that *B. burgdorferi* persists in the human host by transforming into cysts (25) because in vitro studies show that it can alter its morphology under stress conditions such as nutrient deprivation (26). Our real-time imaging captured spirochetes changing into spherical forms, but indirect evidence indicates that they are not bacterial cysts. The image sequences bear substantial similarity to in vitro observations of spirochete ingestion by phagocytes in both morphologic changes (Supplemental Video 6) and the time course for entry of ingested *B. burgdorferi* into phagolysosomes (~20 minutes [ref. 10] vs. 25 minutes in Supplemental Videos 3 and 5). Formation of true bacterial cysts and endospores involves programmatic structural changes that occur over hours to days, not minutes, as we observed (27).

For other bacterial species, phenotypic variants known as "persisters" have been identified based on growth patterns that differ from the bulk of the population and their tolerance to antibiotics (28–30). The study of persisters of biologic relevance is difficult because they are genetically identical to other cells in the population and have a temporary phenotype induced by environmental stress such as antibiotics. In the context of biofilms, this type of persister is thought to contribute to infection relapse when the antibiotic is removed, as these revert to the growth characteristics and antibiotic susceptibility of the original population (28). If the spirochete DNA detected in mouse tissues after antibiotics represents a subpopulation of live spirochetes, this population differs in several ways from persisters studied in other bacterial species. Residual spirochetes, if present, did not revert to cultivable microorganisms once conditions become more favorable to replication, as would be expected to occur when tissues were placed in culture medium. Reversion of a dormant population to an active phenotype was not detected by real-time imaging; motile spirochetes were not seen in tissues of immunodeficient *Myd88*$^{-/-}$ mice at any time point after completion of antibiotics. It is unlikely that spirochetes lost GFP expression because the *gfp* expression cassette in Bb914 is inserted into cp26, a plasmid ubiquitously present in spirochetes and required for viability (15, 31). Although a mutation that would reduce expression could occur in either *gfp* or its *flaB* promoter, it is improbable that spirochetes with such a mutation would also be the only remaining population selectively resistant to antibiotics. If residual amorphous debris noted in the enthesis contained morphologically altered but viable spirochetes, as has been described for an *rpoS* mutant in the tick midgut (32), such forms did not resume the usual spirochete morphology and replicate when placed in culture medium. Importantly, both xenodiagnosis and tissue transplants demonstrated that any spirochetes remaining after antibiotics could not establish infection in the tick or a new mammalian host, even when the recipient mammal was immunocompromised. This is consistent with our previous study

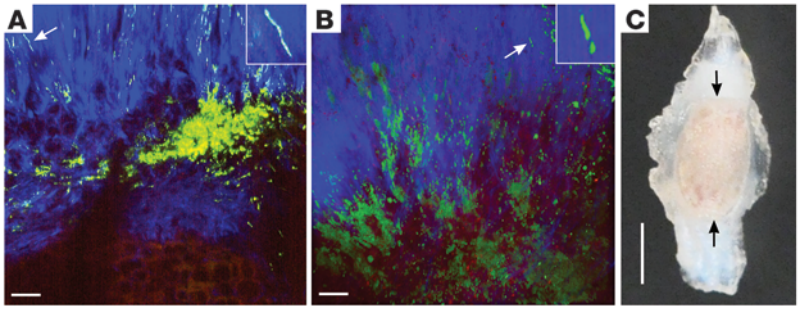

Figure 5
Spirochete remnants persist at the entheses of C3H *Myd88*$^{-/-}$ mice after antibiotic therapy. (**A**) Multiphoton image of Bb914 in patellar tendon (blue) and amorphous GFP deposits at junction of tendon and articular surface (enthesis) of patella (red) of a sham-treated C3H *Myd88*$^{-/-}$ mouse. Arrow indicates region shown in inset. Scale bar: 30 μm. (**B**) Enthesis of a ceftriaxone-treated mouse. Arrow indicates region shown in inset. Scale bar: 30 μm. Images were acquired using a ×20 objective and optically zoomed to a scanned field of view of 300 × 300 μm. The objects delineated by arrows in **A** and **B** are enlarged 3-fold and 4-fold, respectively, in the corresponding insets. (**C**) Photo of articular surface of patella with adjacent tendons. Arrows denote regions where images were acquired. Scale bar: 1 mm.

in which immunosuppression with corticosteroids did not result in positive xenodiagnoses or recrudescence of *B. burgdorferi* infection in WT mice after antibiotic treatment (14).

A recent study in the primate model of Lyme borreliosis reported detection of spirochetes after antibiotic therapy, a conclusion that should be interpreted with caution (33). Subtherapeutic antibiotic levels were documented in experimental animals and measures of infection in the control sham-treated monkeys were not sufficiently robust to distinguish between inadequate treatment and the persistence of a subpopulation with antibiotic tolerance. Furthermore, monkeys were infected by needle inoculation of 3 × 10^8 stationary phase spirochetes, several orders of magnitude greater than the spirochete inoculum size introduced by an *Ixodes* nymph, which is estimated to be in the hundreds (34). Spirochetes are known to lose plasmids and pathogenicity with expansion and serial passaging in vitro (35), and stationary phase cultures used in that study likely comprised a genetically and phenotypically heterogeneous population of organisms. Although phenotypic variants that exhibit antibiotic tolerance may have been introduced into the primates in large numbers and propagated during the 4-month infection period prior to introduction of antibiotics, the study falls short of showing that they can evolve from tick-transmitted spirochetes or low-dose needle inocula in an immunocompetent host.

The finding of fluorescent deposits containing *B. burgdorferi* antigens in the knee entheses after antibiotic treatment has important implications for the pathogenesis of human Lyme arthritis. These deposits have inflammatory potential and can induce TNF-α production from C3H/HeJ macrophages, which are LPS unresponsive (36). Such debris could contribute to prolonged inflammatory responses in the joint after infectious spirochetes have been eradicated. This possibility cannot be addressed in WT or *Myd88*$^{-/-}$ mice because histopathologic evidence of arthritis resolves even though spirochetes persist in the joint for the life span of the infected mouse (10, 14, 37). In humans, treatment-resistant Lyme arthritis has been attributed to localized autoimmunity because *B. burgdorferi* DNA can no longer be detected in synovial fluid or synovectomy tissue (22, 38–40), and immune responses that crossreact with self antigens have been found (41–44). Infection-induced autoimmunity, however, does not explain why this form of arthritis resolves over time, usually within 4 years (3, 45). Recently, a human TLR1 polymorphism (1805GG) that reduces TLR1/2 responsiveness has been

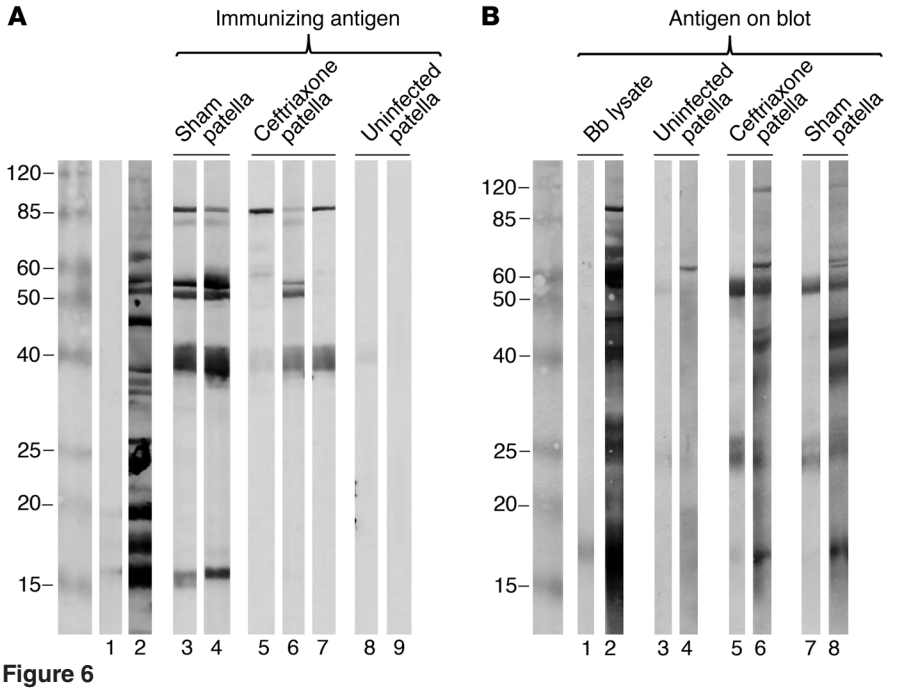

Figure 6
Patella homogenates from antibiotic-treated mice contain *B. burgdorferi* antigens. (**A**) IgG immunoblot of *B. burgdorferi* lysate using sera from mice infected with *B. burgdorferi* or sera from mice immunized with the indicated patella homogenates. All sera were used at 1:100 dilution. Lane 1: normal mouse serum; lane 2: sera from 21-day–infected mice; lanes 3, 4: sera from individual mice immunized with homogenates of patella from sham-treated mice; lanes 5–7: sera from individual mice immunized with homogenates of patellae from ceftriaxone-treated mice; lanes 8, 9: sera from individual mice immunized with homogenates of patella from uninfected mice. (**B**) IgG immunoblot of *B. burgdorferi* lysate or the indicated patella homogenates with normal mouse sera (lanes 1, 3, 5, and 7) or sera from 129-day infected mice (lanes 2, 4, 6, and 8). All sera were used at 1:1,000 dilution.

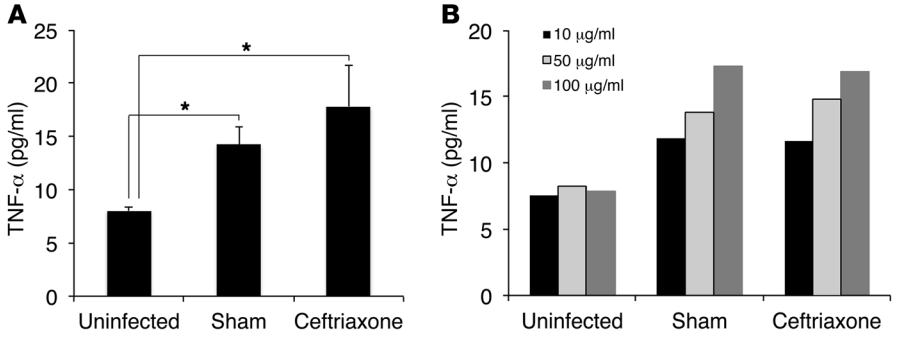

Figure 7

Patellae homogenates from sham- and ceftriaxone-treated mice induce TNF-α production from C3H/HeJ macrophages. (**A**) Macrophages were stimulated with 10 μg/ml of patellae homogenates from the indicated mice. Results represent the mean ± SEM of 4 or more samples from each group. The lower detection limit of the assay was 7.5 pg/ml. *P = 0.0179, Kruskal-Wallis test; $P < 0.05$ for sham versus uninfected and ceftriaxone versus uninfected groups; $P > 0.05$ for sham versus ceftriaxone groups, Dunn's multiple comparisons test. (**B**) Dose response of macrophages to the indicated patellae homogenates. Values of duplicate samples differed by less than 10%.

correlated with greater inflammation after *B. burgdorferi* infection and the development of antibiotic-refractory Lyme arthritis (46). In mice, defects in TLR2 responsiveness lead to elevation in pathogen burden similar to that seen with MyD88 deficiency (9–11). It is possible that the TLR1 polymorphism permits a higher pathogen burden within ligamentous attachments of the joint (regions in humans that have not been sampled for DNA analysis) and that inflammatory spirochete debris remains after antibiotic treatment. Release of foreign antigens could occur as a consequence of biomechanical stress at the entheses and contribute to inflammation at this site and in adjacent synovium. Residual cellular debris that contains spirochete antigens could also perpetuate self responses that might arise during the course of infection, and these would be expected to subside once foreign antigens are eventually cleared.

Persistent musculoskeletal symptoms and/or objective findings (e.g., arthritis) after antibiotic therapy for human Lyme disease have been attributed to host genetic factors, irreversible infection-induced tissue damage, protracted resolution of inflammation, and infection-induced fibromyalgia or autoimmunity (3, 47, 48). Ongoing infection is considered unlikely given the lack of improvement in these complaints with prolonged antibiotic therapy (49–51). Indeed, our real-time imaging has demonstrated that *B. burgdorferi* is highly vulnerable to antibiotics in vivo. Although no single method for detecting viable spirochetes is absolute, the multiple methods applied in this study provide a preponderance of evidence that infectious spirochetes are eliminated. Our studies instead provide what we believe is the first direct evidence that *B. burgdorferi* antigenic and inflammatory debris can persist adjacent to cartilage and articular surfaces in mice for extended periods after antibiotic therapy. Slow degradation of *B. burgdorferi* components at these sites could contribute to the lag in symptom response in patients with disseminated Lyme disease and to the development of antibiotic-resistant Lyme arthritis.

Methods

Mice. Breeding pairs of B6 *Myd88*$^{-/-}$ mice, produced by Shizua Akira (52), were obtained from Joseph Craft (Yale University). Age- and sex-matched B6 WT mice were purchased from the Jackson Laboratories. B6 *Myd88*$^{-/-}$ mice were backcrossed with C3H/HeN mice (Jackson Laboratories) to the F6 generation. Female C3H/HeJ mice (6 to 8 weeks old; Jackson Laboratories) were used as a source of macrophages. *Myd88*$^{-/-}$ mice were maintained as a colony in specific pathogen–free housing with autoclaved food, water, and bedding. Sulfamethoxazole-trimethoprim (0.25 mg/ml; Sulfatrim, Sigma-Aldrich) was added to drinking water to reduce opportunistic infection. Sulfatrim has no effect on *B. burgdorferi* infection or disease and was provided to *Myd88*$^{-/-}$ mice throughout all experiments and to WT mice in experiments comparing WT with *Myd88*$^{-/-}$ mice. Mice were killed by carbon dioxide asphyxiation.

Spirochetes. BbN40 or a GFP-expressing stable transfectant of Bb297 (Bb914) was used (15). Bb914 was provided by Melissa Caimano (University of Connecticut Health Center, Farmington, Connecticut, USA) and exhibits infectivity for mice and ticks similar to that of WT strain 297. Frozen aliquots of low-passage spirochetes were thawed, expanded to log phase in Barbour Stoenner Kelley II medium at 33°C, and then enumerated using a Petroff-Hausser counting chamber. Mice were infected either by infestation with 5 *B. burgdorferi*–infected *Ixodes* nymphs or by intradermal inoculation with 10^4 spirochetes in 100 μl BSK II medium into the interscapular region of the back. The MIC and mean bactericidal concentrations (MBC) of ceftriaxone and doxycycline for each spirochete strain were determined by serial dilution of antibiotics in liquid cultures of *B. burgdorferi* as described (13). For BbN40, the MIC and MBC for doxycycline were 0.5 μg/ml and 4 μg/ml, respectively; the MIC and MBC for ceftriaxone were 0.065 μg/ml and 0.25 μg/ml, respectively. For Bb914, the MIC and MBC for doxycycline were 0.5 μg/ml and 1.0 μg/ml, respectively; the MIC and MBC for ceftriaxone were 0.008 μg/ml and 0.25 μg/ml, respectively.

Tick infestation of mice. Laboratory-reared *Ixodes scapularis* nymphs were provided by Durland Fish (Yale School of Public Health, New Haven, Connecticut, USA). Nymphs infected as described with BbN40 at the larval stage were used to introduce infection into mice (14). Uninfected nymphs were used for xenodiagnosis as described previously (14). From 2 to 5 nymphs were placed on the ears of mice to introduce infection and for xenodiagnoses. Engorged nymphs used for xenodiagnosis were retrieved and housed at 22°C in environmental chambers for up to 8 days prior to analysis.

PCR of B. burgdorferi DNA. DNA was extracted from engorged ticks using either the Allprep DNA/RNA Mini Kit (QIAGEN) or the Isoquick DNA Isolation Kit (Orca Research) according to the manufacturers' protocols. *B. burgdorferi ospA* and *flaB* genes were amplified using the following primer pairs: *ospA* forward 5′-GGTCAAACCACACTTGAAGTT-3′, *ospA* reverse 5′-GTCAGTGTCATTAAGTTC-3′; *flaB* forward 5′-TGTGCCGTTACCTGATTGAA-3′, *flaB* reverse 5′TGCATTAACGCTGCTAATCTT-3′. Robocycler (Stratagene) settings were 35 cycles of 94°C denaturation for 1 minute, 55°C annealing for 1 minute, and 72°C extension for 1 minute followed by a final extension set of 72°C for 10 minutes, yielding product sizes of 332 bp and 255 bp for *ospA* and *flaB* targets, respectively. *I. scapularis* β-*actin* was amplified as a control for DNA amplification from ticks, using the following primer pairs: tick β-*actin* forward 5′-GCCGATGGTCACCTGTCC-3′ and tick β-*actin* reverse 5′-GATGACCCAGATCATGTTGCAGCC-3′ (14). The 400-bp β-*actin* product was amplified under the same parameters as for *ospA* except that the annealing temperature was 59°C and the cycle number was 30. PCR was performed on DNA extracted as described (14) from mouse ear skin, urinary bladders, and knee or tibiotarsal joints. *ospA* was amplified as described above; the *16S rRNA* gene was amplified

using the following primer pair, yielding a 128-bp product: *16S rRNA* forward 5′-TGCTAAGTGTGATGCCTGAAAGAA-3′ and *16S rRNA* reverse 5′-AATCTTTGCCTTCCTCCAACTTATAA-3′. Parameters for *16S rRNA* amplification were identical to those set for the *ospA* gene except that the annealing temperature was 60°C. A 300-bp target of mouse β-*tubulin* was amplified as for the *ospA* gene using the following primer pairs: β-*tubulin* forward 5′-GGCGCCCTCTGTGTAGTGGCCTTTGGCCCA-3′ and β-*tubulin* reverse 5′-CAGGCTGGTCAATGTGGCAACCAGATCGGT-3′.

Antibiotic treatment of mice. Mice were treated with ceftriaxone (16 mg/kg) administered s.c. twice daily for 5 days or a 30-day course of doxycycline administered continuously in water bottles (0.2% doxycycline in drinking water containing 5% sucrose). Control mice were sham treated with 0.9% normal saline s.c. or 5% sucrose in drinking water, respectively. For the 4-months–infected C3H *Myd88*$^{-/-}$ mice, ceftriaxone was administered at the above dose twice daily for 5 days, then daily until sacrifice after 18 days of therapy. Serum doxycycline levels were first optimized in a cohort of mice administered the drug in drinking water. Blood samples were obtained from mice at days 1, 3, and 4 after institution of antibiotics, and drug levels were assessed in triplicate 10-μl serum samples using an agar plate–based bacterial growth inhibition assay with *Staphylococcus aureus* (25923; ATCC) (14). Mice administered oral doxycycline had mean serum levels of 2 ± 0 μg/ml at days 1 and 3 and 1.625 ± 0.25 at day 4. Water bottles containing freshly reconstituted doxycycline were changed every 4 days during the period of antibiotic treatment.

Culture of B. burgdorferi from mouse tissues. Blood, ear skin, and urinary bladders were cultured in BSK II medium as described (5). Cultures were incubated at 33°C and analyzed at 2 weeks for motile spirochetes. Cultures with no growth were held for an additional 15 weeks before they were considered negative.

DFA of ear skin. Ears were flash frozen in OCT and stored at –80°C for group analysis. Cryosections of 6 μm were fixed in acetone and allowed to air dry. After blocking with PBS containing 5% goat serum for 30 minutes or more, sections were stained with FITC-conjugated goat polyclonal Ab to *B. burgdorferi* (1:30 dilution; KPL Inc.) and DAPI (1 μg/ml final concentration; Sigma-Aldrich). Slides were rinsed twice in PBS, then air dried, and coverslips were mounted with Fluoromount-G. Sections were analyzed using an Olympus BX40 widefield immunofluorescence microscope equipped with digital imaging.

Intravital microscopy. Imaging was performed in real time using an upright multiphoton laser scanning microscope. Differences between antibiotic- and sham-treated mice were so marked that it was not possible to blind the imaging personnel to the mouse groups. Images were acquired using an Olympus BX61WI fluorescence microscope with a ×20, 0.95NA water immersion Olympus objective and dedicated single-beam LaVision TriM scanning laser (LaVision Biotec) that was controlled by Imspector software. The microscope was outfitted with a Chameleon Vision II Ti:Sapphire Laser (Coherent) with pulse precompensation. Emission wavelengths of 390–480 nm (blue), 500–550 nm (green, GFP), and 565–665 nm (orange-red) were collected with an array of 3 photomultiplier tubes (Hamamatsu). Mice were anesthetized with an i.p. injection of ketamine (100 mg/kg) and xylazine (10 mg/kg) prior to shaving and Nair application. After prepping, the anesthetized mouse was placed on a custom-designed stereotaxic restraint platform for skin imaging. A plane of deep anesthesia was maintained using a mixture of isoflurane gas and oxygen delivered via a nosecone. For calcaneal tendon imaging, the mouse was immobilized on a stereotactic platform with tweezers to clamp the hip and the spine, and traction was applied to the foot to position the area to be imaged. In some cases, a small incision was made in the skin overlying the tendon to optimize imaging. Patellar entheses images were acquired after mouse euthanasia. Patellae were harvested, and the articular surface of the patella and adjacent rectus femorus and patellar ligaments were imaged immediately. Image stacks of 1 to 61 optical sections with 1- to 2-μm *z*-spacing were acquired every 1 to 25 seconds for 1 to 60 minutes with the laser tuned to a wavelength of 940 nm. Each *xy* plane spanned 300 μm in each dimension with an *xy* resolution of 0.59 μm per pixel. Volocity software (Improvision) was used to create QuickTime-formatted videos of image sequences. All videos are displayed as 2D maximum intensity projections, unless otherwise stated.

Tissue transplant. Cryopreserved ear tissue pieces of 3 mm^2 were transplanted subdermally through a small incision in the back skin of *Myd88*$^{-/-}$ mice anesthetized with ketamine and xylazine. The incision was sealed using surgical glue.

Immunization of mice. *Myd88*$^{-/-}$ mice were immunized by i.p injection with homogenized cryopreserved ear tissue or 80 μg fresh patellae homogenates mixed 1:1 with alum in a total volume of 200 μl. For patellae immunizations, mice were boosted 2 weeks later with 40 μg antigen mixed 1:1 in alum. Sera were analyzed by immunoblot 2 weeks after the last immunization.

Assay for TNF-α production. Patellae harvested aseptically from sham- and ceftriaxone-treated *B. burgdorferi*–infected and uninfected C3H *Myd88*$^{-/-}$ mice (females only) were rinsed twice in tissue homogenization buffer (PBS with 100 U/ml penicillin, 100 μg/ml streptomycin, and 50 μg/ml gentamicin) and then homogenized in 300 μl of buffer on ice. Homogenates were then centrifuged at 828 *g* for 5 minutes to remove particulate debris. The protein concentration in the homogenate supernatants was determined using a modified Bradford assay (Bio-Rad). Splenocytes harvested from female C3H/HeJ mice were resuspended after rbc lysis at 5×10^6/ml in Click's medium supplemented with 10% FBS, 100 U/ml penicillin, 100 μg/ml streptomycin, 2 mM L-glutamine, and 20 μM 2-mercaptoethanol. Splenocytes were aliquoted at 0.5 ml total volume into 24-well plates and incubated for 2 hours at 37°C, after which nonadherent cells were removed by rinsing twice with fresh medium. Adherent macrophages were stimulated with the indicated amounts of protein for 24 hours, after which TNF-α production was assessed by cytokine-specific ELISA according to the manufacturer's recommendations (eBioscience).

B. burgdorferi immunoblot. Proteins in *B. burgdorferi* lysates or patellae homogenates were separated by SDS-PAGE and transferred to nitrocellulose membranes for immunoblot analysis. Membranes were blocked with 3% BSA, after which immunoblots were performed using the indicated dilution of sera and 1:1,000 dilution alkaline phosphatase-conjugated horse anti-mouse IgG (H&L chain–specific) (Vector) as described (10). Bound Ab were visualized by enzymatic reaction with BCIP/NBT phosphatase substrate (KPL).

Statistics. Fisher's exact test was used to assess differences between antibiotic- and sham-treated mouse groups. Differences between TNF-α responses of cells stimulated with uninfected mouse tissue versus tissue that had been infected with *B. burgdorferi* (sham- or antibiotic-treated) were analyzed using the Kruskal-Wallis test with Dunn's multiple comparisons test. *P* values of less than 0.05 were considered significant.

Study approval. Experimental protocols involving mice were approved by the Animal Care and Use Committee at Yale University School of Medicine. All mice were cared for according to Yale Animal Care and Use guidelines.

Acknowledgments

This work was supported by CDC U01 CI000159, NIH P30AR053495, R01AI0857981, and the National Research Fund for Tick-Borne Diseases. The tick colony was maintained with support from Cooperative Agreement 58-0790-2-072 (Durland Fish) from the U.S. Department of Agriculture, Agriculture Research Service. The authors thank Star Dunham-Ems, Melissa Caimano, and Justin Radolf for detailed information regarding the con-

struction and biology of the transformant Bb914. This work was conducted with the excellent technical assistance of Jialing Mao, Ming Li, and Catherine Dailey. We also thank Rebecca L. Fine (current address Williams College) for producing Figure 3F during a Weston High School (Weston, Connecticut, USA) independent study conducted in the Bockenstedt lab and Carmen Booth (Yale Section of Comparative Medicine, New Haven, Connecticut, USA) for the photograph of the patella shown in Figure 5C.

Received for publication October 24, 2011, and accepted in revised form April 24, 2012.

Address correspondence to: Linda K. Bockenstedt, Department of Internal Medicine, Yale University School of Medicine, 300 Cedar Street, New Haven, Connecticut 06520-8031, USA. Phone: 203.785.2454; Fax: 203.785.7053; E-mail: Linda.bockenstedt@yale.edu.

1. Bockenstedt L. Lyme disease. In: Firestein G, Budd R, Harris E Jr, McInnes I, Ruddy S, Sergent J, eds. *Kelley's Textbook of Rheumatology*. St. Louis, Missouri, USA: W.B. Saunders; 2009:1715–1725.
2. Dattwyler RJ, Volkman DJ, Conaty SM, Platkin SP, Luft BJ. Amoxycillin plus probenecid versus doxycycline for treatment of erythema migrans borreliosis. *Lancet*. 1990;336(8728):1404–1406.
3. Steere AC, Angelis SM. Therapy for Lyme arthritis: strategies for the treatment of antibiotic-refractory arthritis. *Arthritis Rheum*. 2006;54(10):3079–3086.
4. Aguero-Rosenfeld ME, Wang G, Schwartz I, Wormser GP. Diagnosis of Lyme borreliosis. *Clin Microbiol Rev*. 2005;18(3):484–509.
5. Barthold SW, Beck DS, Hansen GM, Terwilliger GA, Moody KD. Lyme borreliosis in selected strains and ages of laboratory mice. *J Infect Dis*. 1990; 162(1):133–138.
6. Brown CR, Reiner SL. Genetic control of experimental Lyme arthritis in the absence of specific immunity. *Infect Immun*. 1999;67(4):1967–1973.
7. Brown CR, Reiner SL. Bone-marrow chimeras reveal hemopoietic and nonhemopoietic control of resistance to experimental Lyme arthritis. *J Immunol*. 2000;165(3):1446–1452.
8. Barthold SW, Sidman CL, Smith AL. Lyme borreliosis in genetically resistant and susceptible mice with severe combined immunodeficiency. *Am J Trop Med Hyg*. 1992;47(5):605–613.
9. Bolz DD, et al. MyD88 plays a unique role in host defense but not arthritis development in Lyme disease. *J Immunol*. 2004;173(3):2003–2010.
10. Liu N, Montgomery RR, Barthold SW, Bockenstedt LK. Myeloid differentiation antigen 88 deficiency impairs pathogen clearance but does not alter inflammation in *Borrelia burgdorferi*-infected mice. *Infect Immun*. 2004;72(6):3195–3203.
11. Wang G, Ma Y, Buyuk A, McClain S, Weis JJ, Schwartz I. Impaired host defense to infection and Toll-like receptor 2-independent killing of *Borrelia burgdorferi* clinical isolates in TLR2-deficient C3H/HeJ mice. *FEMS Microbiol Lett*. 2004; 231(2):219–225.
12. Yrjanainen H, Hytonen J, Song XY, Oksi J, Hartiala K, Viljanen MK. Anti-tumor necrosis factor-alpha treatment activates *Borrelia burgdorferi* spirochetes 4 weeks after ceftriaxone treatment in C3H/He mice. *J Infect Dis*. 2007;195(10):1489–1496.
13. Hodzic E, Feng S, Holden K, Freet KJ, Barthold SW. Persistence of *Borrelia burgdorferi* following antibiotic treatment in mice. *Antimicrob Agents Chemother*. 2008;52(5):1728–1736.
14. Bockenstedt LK, Mao J, Hodzic E, Barthold SW, Fish D. Detection of attenuated, noninfectious spirochetes in *Borrelia burgdorferi*-infected mice after antibiotic treatment. *J Infect Dis*. 2002; 186(10):1430–1437.
15. Dunham-Ems SM, et al. Live imaging reveals a biphasic mode of dissemination of *Borrelia burgdorferi* within ticks. *J Clin Invest*. 2009;119(12):3652–3665.
16. Pavia C, Inchiosa MA Jr, Wormser GP. Efficacy of short-course ceftriaxone therapy for *Borrelia burgdorferi* infection in C3H mice. *Antimicrob Agents Chemother*. 2002;46(1):132–134.
17. Harman M, et al. The heterogeneous motility of the Lyme disease spirochete in gelatin mimics dissemination through tissue. *Proc Natl Acad Sci U S A*. 2012; 109(8):3059–3064.
18. Wormser GP, et al. *Borrelia burgdorferi* genotype predicts the capacity for hematogenous dissemination during early Lyme disease. *J Infect Dis*. 2008; 198(9):1358–1364.
19. Steere AC, Grodzicki RL, Craft JE, Shrestha M, Kornblatt AN, Malawista SE. Recovery of Lyme disease spirochetes from patients. *Yale J Biol Med*. 1984; 57(4):557–560.
20. Ambrose PG, et al. Pharmacokinetics-pharmacodynamics of antimicrobial therapy: it's not just for mice anymore. *Clin Infect Dis*. 2007;44(1):79–86.
21. Wormser GP, Schwartz I. Antibiotic treatment of animals infected with *Borrelia burgdorferi*. *Clin Microbiol Rev*. 2009;22(3):387–395.
22. Li X, McHugh GA, Damle N, Sikand VK, Glickstein L, Steere AC. Burden and viability of *Borrelia burgdorferi* in skin and joints of patients with erythema migrans or Lyme arthritis. *Arthritis Rheum*. 2011;63(8):2238–2247.
23. Young G, Turner S, Davies JK, Sundqvist G, Figdor D. Bacterial DNA persists for extended periods after cell death. *J Endod*. 2007;33(12):1417–1420.
24. Brundin M, Figdor D, Roth C, Davies JK, Sundqvist G, Sjogren U. Persistence of dead-cell bacterial DNA in ex vivo root canals and influence of nucleases on DNA decay in vitro. *Oral Surg Oral Med Oral Pathol Oral Radiol Endod*. 2010;110(6):789–794.
25. Miklossy J, Kasas S, Zurn AD, McCall S, Yu S, McGeer PL. Persisting atypical and cystic forms of *Borrelia burgdorferi* and local inflammation in Lyme neuroborreliosis. *J Neuroinflammation*. 2008;5:40.
26. Alban PS, Johnson PW, Nelson DR. Serum-starvation-induced changes in protein synthesis and morphology of *Borrelia burgdorferi*. *Microbiology*. 2000; 146(pt 1):119–127.
27. Sonenshein AL. Endospore-forming bacteria, an overview. In: Brun Y, Shimkets L, eds. *Prokaryotic Development*. Washington, DC, USA: ASM Press; 2000:133–150.
28. Lewis K. Multidrug tolerance of biofilms and persister cells. *Curr Top Microbiol Immunol*. 2008; 322:107–131.
29. Lewis K. Persister cells. *Annu Rev Microbiol*. 2010; 64:357–372.
30. Dawson CC, Intapa C, Jabra-Rizk MA. "Persisters": survival at the cellular level. *PLoS Pathog*. 2011; 7(7):e1002121.
31. Byram R, Stewart PE, Rosa P. The essential nature of the ubiquitous 26-kilobase circular replicon of *Borrelia burgdorferi*. *J Bacteriol*. 2004; 186(11):3561–3569.
32. Dunham-Ems SM, Caimano MJ, Eggers CH, Radolf JD. *Borrelia burgdorferi* requires the alternative sigma factor RpoS for dissemination within the vector during tick-to-mammal transmission. *PloS Pathog*. 2012;8(2):e1002532.
33. Embers ME, et al. Persistence of *Borrelia burgdorferi* in Rhesus Macaques following antibiotic treatment of disseminated infection. *PLoS One*. 2012; 7(1):e29914.
34. Ohnishi J, Piesman J, de Silva AM. Antigenic and genetic heterogeneity of *Borrelia burgdorferi* populations transmitted by ticks. *Proc Natl Acad Sci U S A*. 2001;98(2):670–675.
35. Schwan TG, Burgdorfer W, Garon CF. Changes in infectivity and plasmid profile of the Lyme disease spirochete, *Borrelia burgdorferi*, as a result of in vitro cultivation. *Infect Immun*. 1988;56(8):1831–1836.
36. Poltorak A, et al. Defective LPS signaling in C3H/HeJ and C57BL/10ScCr mice: mutations in TLR4 gene. *Science*. 1998;282(5396):2085–2088.
37. Barthold SW, de Souza MS, Janotka JL, Smith AL, Persing DH. Chronic Lyme borreliosis in the laboratory mouse. *Am J Pathol*. 1993;143(3):959–971.
38. Bradley JF, Johnson RC, Goodman JL. The persistence of spirochetal nucleic acids in active Lyme arthritis. *Ann Intern Med*. 1994;120(6):487–489.
39. Carlson D, Hernandez J, Bloom BJ, Coburn J, Aversa JM, Steere AC. Lack of *Borrelia burgdorferi* DNA in synovial samples from patients with antibiotic treatment-resistant Lyme arthritis. *Arthritis Rheum*. 1999;42(12):2705–2709.
40. Priem S, Burmester GR, Kamradt T, Wolbart K, Rittig MG, Krause A. Detection of *Borrelia burgdorferi* by polymerase chain reaction in synovial membrane, but not in synovial fluid from patients with persisting Lyme arthritis after antibiotic therapy. *Ann Rheum Dis*. 1998;57(2):118–121.
41. Gross DM, et al. Identification of LFA-1 as a candidate autoantigen in treatment-resistant Lyme arthritis. *Science*. 1998;281(5377):703–706.
42. Steere AC, Falk B, Drouin EE, Baxter-Lowe LA, Hammer J, Nepom GT. Binding of outer surface protein A and human lymphocyte function-associated antigen 1 peptides to HLA-DR molecules associated with antibiotic treatment-resistant Lyme arthritis. *Arthritis Rheum*. 2003;48(2):534–540.
43. Steere AC, et al. Antibiotic-refractory Lyme arthritis is associated with HLA-DR molecules that bind a *Borrelia burgdorferi* peptide. *J Exp Med*. 2006; 203(4):961–971.
44. Ghosh S, Seward R, Costello CE, Stollar BD, Huber BT. Autoantibodies from synovial lesions in chronic, antibiotic treatment-resistant Lyme arthritis bind cytokeratin-10. *J Immunol*. 2006;177(4):2486–2494.
45. Steere AC, Schoen RT, Taylor E. The clinical evolution of Lyme arthritis. *Ann Intern Med*. 1987; 107(5):725–731.
46. Strle K, Shin JJ, Glickstein LJ, Steere AC. Association of a Toll-like receptor 1 polymorphism with heightened Th1 inflammatory responses and antibiotic-refractory Lyme arthritis. *Arthritis Rheum*. 2012; 64(5):1497–1507.
47. Wormser GP, et al. The clinical assessment, treatment, and prevention of Lyme disease, human granulocytic anaplasmosis, and babesiosis: clinical practice guidelines by the Infectious Diseases Society of America. *Clin Infect Dis*. 2006;43(9):1089–1134.
48. Feder HM Jr, et al. A critical appraisal of "chronic Lyme disease". *N Engl J Med*. 2007;357(14):1422–1430.
49. Klempner MS, et al. Two controlled trials of antibiotic treatment in patients with persistent symptoms and a history of Lyme disease. *N Engl J Med*. 2001; 345(2):85–92.
50. Krupp LB, et al. Study and treatment of post Lyme disease (STOP-LD): a randomized double masked clinical trial. *Neurology*. 2003;60(12):1923–1930.
51. Fallon BA, et al. A randomized, placebo-controlled trial of repeated IV antibiotic therapy for Lyme encephalopathy. *Neurology*. 2008;70(13):992–1003.
52. Adachi O, et al. Targeted disruption of the MyD88 gene results in loss of IL-1-and IL-18-mediated function. *Immunity*. 1998;9(1):143–150.